Crystal structure prediction and first-principles investigation of the vibrational, electronic, and optical properties of yttrium oxyhydride

Bachelor's Thesis

Student: Ivan Novoseltsev
Student code: 233137YAFB
Supervisor: Mihhail Klopov, Associate Professor, Department of Physics, Institute of Cybernetics
Co-supervisor: Smagul Karazhanov, Leading Researcher,
Thin Film Laboratories, Institute of Solid State Physics, University of Latvia, Riga, Latvia
Curriculum: Applied Physics

Tallinn 2026

Ütriumoksühüdriidi kristallstruktuuri ennustamine ning vibratsiooniliste, elektrooniliste ja optiliste omaduste uurimine esimeste printsiipide alusel

Bakalaureusetöö

Üliõpilane: Ivan Novoseltsev
Üliõpilaskood: 233137YAFB
Juhendaja: Mihhail Klopov, Dotsent, Füüsika osakond, Küberneetika instituut
Kaasjuhendaja: Smagul Karazhanov, Juhtivteadur,
Õhukeste kilede laboratoorium, Läti Ülikool, Tahkisefüüsika Instituut, Riia, Läti
Õppekava: Rakendusfüüsika

Tallinn 2026

Declaration

I hereby declare that I have written this thesis independently and the thesis has not previously been submitted for defence. All works and major viewpoints of the other authors, data from sources of literature and elsewhere used for writing this paper have been properly cited.

Author: Ivan Novoseltsev

The thesis complies with the requirements for bachelor's theses.

Supervisors: Mihhail Klopov, Smagul Karazhanov

Contents

Glossary of abbreviations and terms

Å	Angstrom (unit of length)
DFT	Density functional theory
DOS	Density of states
eV	Electronvolt
FCC	Face-centered cubic lattice
GGA	Generalized gradient approximation
HSE06	Heyd-Scuseria-Ernzerhof hybrid functional
k-point	Point in reciprocal space used for Brillouin zone sampling
PAW	Projector augmented-wave method
PBE	Perdew-Burke-Ernzerhof exchange-correlation functional
PDOS	Projected density of states
Phonon	Quantised lattice vibration
phonopy	Phonon calculation package
SCF	Self-consistent field
VASP	Vienna Ab initio Simulation Package
YHO	Yttrium oxyhydride

VASP input and output files

CHGCAR	File storing the electronic charge density
CONTCAR	File describing the relaxed crystal structure
INCAR	Input file controlling calculation parameters
KPOINTS	File defining Brillouin zone k-point sampling
POSCAR	File describing the crystal structure (lattice and atomic positions)
POTCAR	File containing pseudopotentials (PAW datasets)
WAVECAR	File storing electronic wavefunctions

1 Introduction

1.1 Motivation

Recently, there has been significant interest in the development of so-called functional (or “smart”) materials with predetermined physical properties [1]. The aim of this work is to demonstrate a method for predicting new stable crystalline structures, followed by an analysis of their physical properties. This study investigates a photochromic yttrium oxyhydride crystal, whose absorption properties change upon exposure to ultraviolet radiation [2]. The development of functional materials is complicated by the fact that, for a given chemical composition, the crystal structure is not known in advance, and for one set of chemical elements there may exist many different atomic configurations (structures). Exhaustive enumeration of all variants is extremely difficult and impractical, since a significant fraction of structures is energetically unstable or their properties are not of interest. Experimental methods do not allow a systematic exploration of the full set of possible configurations and are typically applied to already selected candidates. This creates a need for a method that allows the construction and selection of physically reasonable structures, followed by their analysis using density functional theory (DFT) [3, 4] to analyse their physical properties. This problem is one of the key challenges in modern materials science, as it enables the transition from empirical material discovery to the design of materials with desired properties. The novelty of this work lies in the application of an approach that combines the generation of crystal structures based on symmetry with subsequent analysis of their physical properties.

1.2 Functional materials

The development and study of such materials is a promising direction in modern science. Of particular interest are structures with increased chemical complexity, such as mixed-anion materials, due to the multiple interactions between different atoms within these structures. Thus, combining different types of interactions allows the targeted design of materials with unique properties for specific applications.

Despite their high potential, this field remains insufficiently explored due to the difficulty of predicting the behavior of multicomponent systems (high dimensionality of chemical space, multiscale interactions), limited accuracy of theoretical models, as well as the fact that experimental investigation of such materials is associated with challenges in synthesizing homogeneous samples, complex structural and spectroscopic characterization methods, and the high cost and long duration of cycles: “synthesis, analysis, optimisation”.

1.3 Importance of crystal structure prediction

Crystalline compounds are materials with an ordered atomic structure described by a space group and lattice type [5]. They are used as a basis for functional materials because their ordered atomic structure ensures a predictable and controllable distribution of electrons. A periodic lattice allows accurate modeling of material behavior and enables targeted control of functionality. In contrast to amorphous systems, crystalline structures exhibit high thermodynamic stability and reproducibility of properties, which is critical, for example for industrial applications.

The same chemical composition can correspond to many different crystal structures due to the existence of multiple local energy minima. Some of these structures may be stable, others unstable, and others metastable (the compound is in a local, but not global, energy minimum; it is thermodynamically unstable and may transform into a more stable state with less energy, but it can be experimentally realised and may have practical applications). Knowledge of composition alone is not sufficient to construct such structures; other parameters must also be considered, such as lattice parameters (a, b, c) and angles (α, β, γ), space group, type of chemical bonding, distribution of atoms and defects in the lattice, electronic structure, and synthesis conditions (temperature, pressure). Before designing new structures, it is necessary to determine which structures are physically realisable under given conditions and constraints.

Knowledge of these parameters makes it possible to establish a direct relationship between chemical composition and functional behavior, which enables the prediction of crystal structures and, consequently, the investigation of materials with desired properties.

1.4 Methods for predicting new crystalline structures

Various methods are used to predict crystal structures, depending on the type of problem, including molecular dynamics [6], global optimisation algorithms [7], and machine learning [8]. However, these methods have limitations in terms of computational cost, efficiency in locating the energy minimum, and dependence on input data, which are impractical in this case.

The method that overcomes the above-mentioned difficulties is a symmetry-based approach [9–11]. Within this method, candidate crystal structures are constructed as follows: atoms corresponding to the desired chemical composition are placed on symmetry-allowed positions within crystallographic space groups (Wyckoff positions [5, 12]). This procedure significantly reduces the number of possible configurations. The resulting structures are then analysed using first-principles calculations implemented in the Vienna Ab initio Simulation Package (*VASP*) [13, 14] based on density functional theory, allowing a reliable determination of the structural stability, as well as the electronic and optical properties.

1.5 Aim of the thesis

The aim of this work is to investigate yttrium oxyhydride (YHO) and to establish the relationship between its atomic structure and physical properties using density functional theory (DFT).

The following tasks are addressed:

- construction of the YHO crystal structure based on symmetry analysis,
- geometry optimisation,
- analysis of the dynamical stability,
- calculation of the electronic structure and density of states (DOS),
- investigation of optical properties,
- comparison of the calculated properties with experimental data.

2 Literature review

2.1 Transition and rare-earth elements

Transition elements are characterised by the gradual filling of the d-electron shell, which is empty in alkaline-earth metals and completely filled in noble metals ($3d$, $4d$, $5d$)[1] [15]. The presence of electrons in these shells influences properties such as chemical bonding, electrical conductivity, and the magnetic and optical behaviour of materials [16]. Since a single d-shell can accommodate up to 10 electrons, transition metals are characterised by a high density of electronic states (DOS), which contributes to enhanced magnetic effects and paramagnetic susceptibility [16]. At the same time, d-electrons strongly interact with the crystal field created by neighbouring ions [16].

Rare-earth elements represent a group of chemically similar metals including scandium (Sc), yttrium (Y), and the lanthanides [17]. A characteristic feature of these elements are the presence of $4f$-electron shells, the number of electrons in which gradually increases across the lanthanide series [16, 17]. These shells play an important role in determining the magnetic and electronic properties of materials [15, 16]. In contrast to the d-electrons of transition metals, $4f$-electrons are strongly localised and situated deep inside the ion. As a result, the magnetic properties of rare-earth ions are less sensitive to the crystal environment than those of transition metals [16].

2.2 Mixed-anion systems

Mixed-anion systems are materials containing several different anions within the same structure [18]. Since different anions differ in charge, ionic radius, electronegativity, and polarisability, their interactions with each other and with the metallic cation give rise to unusual properties inaccessible to conventional single-anion systems [18, 19]. Changing the anion composition affects the electronic structure, band gap, chemical bonding, crystal symmetry, and optical properties of the material.

Several types of mixed-anion systems are have been studied, including oxyfluorides (containing O^{2-} and F^{-}), oxynitrides (O^{2-}, N^{3-}), chalcohalides (S^{2-} and Cl^{-}), and oxyhydrides (O^{2-} and H^{-}). Changing the composition makes it possible to obtain compounds with new or improved properties and acn also help stabilise structures [20].

Oxyhydrides are a particularly interesting subgroup of mixed-anion materials, since they contain two different anions: O^{2-} and H^{-}. The behaviour of the hydride ion is significantly different both from the ordinary state of hydrogen (H^{+} in water and acids) and from most common anions in terms of chemical bonding and influence on the electronic structure, since it does not possess p orbitals in the valence shell; its electronic configuration is $1s^2$. H^{-} can participate in several different types of bonding depending on the neighbouring atoms: ionic, covalent, and metallic bonding [18]. By modifying the composition of the oxyhydride, it becomes possible to control the properties of the

[1] A fourth $6d$ transition-metal series (Lr–Cn) is also expected, although it consists of superheavy synthetic elements with mostly predicted electronic configurations and is rarely discussed in conventional materials science.

hydride anion, which affects the behaviour of the whole compound.

Rare-earth and transition elements easily react with hydrogen to form hydrides [17]. Upon interaction with air, such hydrides oxidise, forming thin oxyhydride films. A characteristic feature of this subgroup of oxyhydrides is reversible photochromism, a change in optical properties (darkening and transparency change) under illumination [2]. In contrast, the parent hydride itself does not exhibit such behaviour, which emphasises the importance of the simultaneous presence of both oxide and hydride anions in this process. Similarly to the choice of anions, the choice of metallic cation also changes the material properties; experimental studies have demonstrated variations in the band gap for different rare-earth metals [17].

The listed properties and the possibility of tuning them open opportunities for practical applications of mixed-anion systems, including smart windows, energy-efficient coatings, optical devices, and energy storage and conversion technologies [17, 18].

2.3 Yttrium oxyhydride system

The yttrium oxyhydride system (Y-H-O) belongs to the class of mixed-anion compounds, as it contains both O^{2-} and H^{-}, which is atypical for conventional solid-state compounds. The unusual optical properties of this system result from this configuration.

The first key work in this field is “A new thin film photochromic material: Oxygen-containing yttrium hydride” by Mongstad et al. (2011) [2]. In this work, thin films of yttrium hydride were investigated, and upon contact with air, unusual properties were observed, such as transparency and photochromism (a reversible colour change under visible light). These effects were caused by the interaction with oxygen molecules, which led to the suggestion that the obtained compound was not a pure hydride. This work indicated the possible existence of a Y-H-O system, which was a combination of yttrium hydride (YH_x) and oxygen. Further investigation of the formation conditions and the phase nature was required.

The next work, by Montero et al., “Preparation of yttrium hydride-based photochromic films by reactive magnetron sputtering” (2018) [21] was dedicated to studying the synthesis mechanism of this compound. Synthesis consisted of two subsequent stages: formation of a yttrium hydride (YH_x) and later oxidation of this hydride, resulting in the formation of YH_xO_y. The results were obtained using X-ray photoelectron spectroscopy (XPS) and energy-dispersive X-ray spectroscopy (EDS) to analyse the chemical composition, and X-ray diffraction (XRD) was used to determine the crystal structure. It was confirmed that oxygen is incorporated into the lattice of the hydride, while the face-centered cubic (fcc) symmetry remains, with a change in the lattice parameters. No separate oxide phase was observed. However, the nature of the resulting phase remained unclear, leaving open the question of whether the material is a mixture of phases or a new compound.

The next important step was related to the study of the chemical nature of this compound. The work of Cornelius et al. “Oxyhydride Nature of Rare-Earth-Based Photochromic Thin Films” (2019) [22] showed that the system contains two types of anions simultaneously: O^{2-} and H^{-} ions. It has been

proven that this compound cannot be described as a mixture of phases, but as a single-phase mixed-anion compound. In this publication, the term “oxyhydride” was introduced to describe such systems.

After clarifying the chemical nature, the next objective was to determine the precise structure of the compound. Under the supervision of Sørby, the work titled “On the Crystal Chemistry of Photochromic Yttrium Oxyhydride” (2022) [23] was published. In this wotk, neutron diffraction (a method sensitive to lightweight atoms, such as hydrogen) was used to determine lattice parameters and atomic positions. It was shown that hydrogen and oxygen atoms occupy the same interstitial positions, referred to as tetrahedral sites. This confirmed the result reported by Montero et al. (2016), indicating the fcc structure. This work experimentally established that YHO is a well-defined oxyhydride phase.

3 Methodology

3.1 Overview of crystal structure prediction methods

Several different methods are used for predicting crystal structures. They differ greatly from each other, and each method has its own disadvantages and advantages. The method for structure prediction is selected depending on the goals of the study.

The most straightforward approach is the experimental synthesis. It consists in attempting to create the desired structure under laboratory conditions. This method is often limited in its application because of its high cost, the complexity of the implementation conditions, and the difficulty of obtaining the full range of theoretically possible configurations. Therefore, in order to avoid the above-mentioned problems, systematic screening and analysis of structures based on computational processes are often used, since this is faster, more accessible, and provides more complete and detailed results.

One of the computational methods is molecular dynamics (MD) simulation, the essence of which lies in modelling the evolution of atoms, after which thermodynamically possible candidates are selected. This method takes a great deal of time and may fail to find the true global energy minimum.

A more detailed investigation is achieved using global optimisation algorithms. Evolutionary methods are one representative of this approach. One of the programs of this kind is *USPEX* [7]. Evolutionary methods generate populations of structures (sets of different crystal configurations with the same composition, considered as possible solutions at each step of the evolutionary search) and iteratively improve the selection of candidates through crossover and mutations, imitating real evolution. In a similar way, the particle swarm optimisation (PSO) method implemented in *CALYPSO* [24] treats structures as particles moving in configuration space and guided by both individual and collective experience in order to adjust particle motion towards low-energy configurations. “Experience” in this context means the information accumulated during the search process: individual experience is the best position reached by a particle, and collective experience is the best position found by the entire population. Another widely used approach is *AIRSS* [25], which is based on generating a large number of random structures and selecting the energetically favourable ones among them, which is fast, but not always reliable.

In recent years, machine learning has found application in many fields of science for accelerating calculations and finding new solutions, and materials science is no exception. Machine-learned potentials model the energy distribution on the basis of training data, which makes it possible to evaluate promising structures rapidly. However, despite the broad possibilities, the application of this method depends very strongly on the quality, size, and transferability of the data (transferability is the ability of a model trained on one set of data to generalise to others), which limits the use of machine learning for behaviourally complex and less studied systems.

First-principles calculations (ab initio calculations) are based on density functional theory (DFT [3,

4]) and are capable of describing materials without empirical parameters, relying on quantum-mechanical principles. Although they require substantial computational cost, they make it possible to evaluate structural stability, electronic structure, and related physical properties. The calculations are performed without relying on empirical data, which makes it possible to evaluate and verify candidate structures, providing broad opportunities for the search for new materials.

In this work, the latter method is used for the analysis of candidate structures, namely first-principles calculations implemented in *VASP*. Using this program package, such processes as structure optimisation and the subsequent investigation of its properties are carried out (density of states (DOS, the number of quantum states per unit energy), dynamical stability through phonon calculations, and optical properties). This choice is motivated by the need for reliable and verifiable results in the system under study, where the available data are limited, but an accurate description of the electronic and optical properties is required. The procedure used for candidate structure construction is described in Section 3.2.

3.2 Structure construction procedure

Structure construction can be performed using a symmetry-based approach involving space groups, Wyckoff positions, and subgroup relations [5, 12, 19, 20].

The construction procedure consists of selecting a parent crystal structure (preferably with high symmetry), analysing its Wyckoff positions, interstitial sites and possible substitutions, and modifying the occupation of symmetry-equivalent atomic sites in order to generate ordered crystal structures.

Ordered substitutions of equivalent crystallographic positions may reduce the symmetry of the parent structure and lead to the formation of a crystallographic subgroup of the parent space group. Such modifications include atomic permutations, displacements, rotations, reflections and occupancy changes performed under symmetry constraints. The imposed symmetry constraints substantially reduce the number of independent structural degrees of freedom and limit the search space to crystallographically allowed configurations. After abovementioned operations, number of new crystallographically reasonable candidate structures are obtained, which is much smaller than the one obtained with simple exhaustive search.

In the present work, the procedure was applied to fcc-derived structures relevant for rare-earth hydrides and oxyhydrides. After constructing the crystallographic model, the corresponding periodic unit cell was generated and converted into a representation suitable for first-principles calculations. For cubic structures, the conventional lattice vectors are given by

$$\vec{A}_1 = (a, 0, 0), \quad \vec{A}_2 = (0, a, 0), \quad \vec{A}_3 = (0, 0, a), \tag{1}$$

where a is the conventional lattice parameter. For fcc structures, the primitive lattice vectors can be obtained from the conventional cubic cell as

$$\vec{a}_1 = \frac{1}{2}(\vec{A}_2 + \vec{A}_3), \quad \vec{a}_2 = \frac{1}{2}(\vec{A}_1 + \vec{A}_3), \quad \vec{a}_3 = \frac{1}{2}(\vec{A}_1 + \vec{A}_2), \tag{2}$$

which gives

$$\vec{a}_1 = (0, a/2, a/2), \quad \vec{a}_2 = (a/2, 0, a/2), \quad \vec{a}_3 = (a/2, a/2, 0). \tag{3}$$

The primitive representation reduces the number of atoms in the simulation cell while preserving the translational symmetry of the lattice, which decreases the computational cost of DFT calculations. Additional details of the fcc translation vectors are provided in Appendix A.

The generated structures are subsequently converted into *VASP* input files (POSCAR), optimised using DFT calculations and tested for stability.

3.3 Computational details

3.3.1 Density Functional Theory

Density functional theory (DFT) is a quantum-mechanical method for electronic structure calculation in multielectron systems. The main idea of the theory is to replace many-electron wavefunction with electron density. It simplifies calculations, because the wavefunction depends on 3N spatial variables, and the electron density depends only on three spatial variables.

In practical calculations, the Kohn-Sham formalism is used, in which electrons of the system are treated as non-interacting. All interactions are described through an effective potential. The effective potential includes: the potential of atomic nuclei, Coulomb interaction and exchange-correlation contribution (quantum effects of electron interactions).

The main limitation of DFT is that the exact form of the exchange-correlation functional is unknown. In practice, it is approximated using parameterisations based on accurate reference data, such as quantum Monte Carlo calculations of the homogeneous electron gas [26]. This leads to commonly used functionals, such as the local density approximation (LDA) [27] and generalized gradient approximation (GGA) [28]. More advanced approaches, such as double-hybrid functionals [29] (MP2 [30]), also exist, but are not used in the present work.

In this work, the generalised gradient approximation (GGA) is used, specifically the Perdew-Burke-Ernzerhof (PBE) functional [31]. PBE provides good enough accuracy and, at the same time, low computation cost. This is the reason for which PBE is widely used in solving problems in solid-state physics.

To reduce the computational cost, core electrons can be replaced by an effective core potential, and only valence electrons are treated explicitly. This is achieved using pseudopotentials (or the projector augmented-wave (PAW) method in *VASP*) [32, 33].

Now, DFT still has several problems, including the inaccurate description of intermolecular interactions such as van der Waals forces [34] and the underestimation of band gaps.To improve accuracy of electron localisation and band gap calculations, hybrid functionals are used, such as Heyd-Scuseria-Ernzerhof (HSE) [35]. This is a combination of full-electron calculations and DFT.

3.3.2 Software and implementation

Vienna Ab initio Simulation Package (*VASP*) is a software package based on DFT, used for ab initio calculations in solid-state physics. *VASP* uses the Vanderbilt pseudopotentials or the PAW method with a plane-wave basis set. In this work, the PAW method is used. Such methods allow the calculation of structural properties (lattice parameters, atomic positions), electronic and optical properties, and phonon spectra. *VASP* supports different exchange-correlation functionals such as PBE (used as the main functional), hybrid functionals (HSE), and also advanced methods, such as GW [36] (Green's function and screened Coulomb interaction) and RPA (random phase approximation) [37, 38]. In this work, two functionals are used: PBE for initial calculations and HSE06 [39] (a parametrisation form of HSE) to obtain more accurate electronic and optical properties.

Crystal structure was visualised using the *VESTA* software [40]. The *phonopy* package was used together with *VASP* for phonon calculations and vibrational property analysis [41]. Electronic density of states and optical spectra were processed and plotted using the *sumo* package [42].

The *ChatGPT* [43] artificial intelligence tool was used for language correction, formatting assistance, and support in searching for literature sources.

3.4 Structure optimisation procedure

In ab initio calculations, geometry optimisation must be performed prior to the analysis of physical properties, both when using structures obtained from databases and when constructing structures manually. If a structure is acquired from an external database, additional optimisation is required to ensure consistency between all calculations. The original calculations may have been performed using different exchange-correlation functionals, accuracy settings, pseudopotentials, k-point meshes, and other computational parameters. Re-optimisation allows all investigated structures to be brought to the same computational conditions before further analysis of their properties. If the structure is instead created manually from the start or generated from parent compounds (in the present work, from yttrium dihydride), the initial atomic configuration generally does not correspond to the equilibrium state of the system. Such a structure may contain non-equilibrium interatomic distances, internal stresses, and non-optimised atomic coordinates. Therefore, geometry optimisation is necessary in order to obtain a physically stable structure suitable for further calculations.

Structure optimisation is the process of searching for equilibrium atomic configurations while simultaneously minimising the total energy of the compound in order to obtain an energetically stable state of the system. An equilibrium atomic configuration corresponds to a state in which the forces acting on atoms approach zero. The total energy of the system is the sum of all kinetic and potential energy contributions of its constituent particles. According to the second Hohenberg-Kohn theorem, the total energy of a system is a functional of the electron density and reaches its minimum for the true ground-state electron density [3].

The minimisation of the total energy during geometry optimisation is achieved through the sequential solution of the electronic and ionic subsystems. For a fixed atomic configuration, the electronic structure is calculated iteratively within the framework of the SCF procedure. At each step, an effective electronic potential depending on the current electron density distribution is constructed, after which the single-electron Kohn-Sham equations [4] are solved in order to obtain updated electronic states. A new electron density is then constructed from these states, and the cycle is repeated until a self-consistent solution is reached, for which the changes in the total energy and electron density between iterations become smaller than the specified convergence criteria [3].

After electronic convergence is achieved, the forces acting on the atoms are calculated and used to update the atomic coordinates. The electronic structure is then recalculated for the new geometry, and this cycle is repeated until an equilibrium configuration of the system is reached. The relation between total-energy minimisation and atomic forces is defined by the fact that the forces correspond to the negative gradient of the total energy E_{tot} of the system with respect to the atomic coordinates R_i:

$$F_i = -\frac{\partial E_{\text{tot}}}{\partial R_i}. \tag{4}$$

This means that the forces indicate the direction of the steepest decrease in the total energy and determine atomic displacements during optimisation. As the structure relaxes, the residual forces decrease and the system approaches a local minimum on the potential energy surface. In addition to the atomic forces, the residual stress of the lattice is also analysed after optimisation, which characterises the mechanical equilibrium of the unit cell.

Geometry optimisation may involve different degrees of freedom depending on the purpose of the calculation. In the simplest case, only the atomic coordinates are optimised while the lattice vectors remain fixed. Such an approach is commonly used in the investigation of local structural defects, where the unit-cell parameters are already known and do not require additional relaxation. In the more general case, the shape and volume of the lattice are optimised together with the atomic positions. This makes it possible to determine the equilibrium geometry of the structure, which is necessary for crystal structure prediction. In this work, optimisation of both the lattice parameters and atomic positions was performed.

An important concept in geometry optimisation is the potential energy surface (PES) [44]. The PES describes a multidimensional energy landscape in which different atomic configurations correspond to different values of the total energy and multiple local minima may exist. During the optimisation process, the algorithm searches for the nearest local minimum. Therefore, the obtained result depends on the initial geometry of the structure. Different local minima correspond to stable or metastable states of the same compound, indicating the possibility of several crystalline phases or structural modifications with different atomic arrangements and symmetries.

Optimisation algorithms in DFT are numerical minimisation methods that search for the minimum-energy configuration on the PES. Conjugate-gradient and quasi-Newton methods are commonly used approaches for geometry relaxation [45]. These algorithms use energy gradients (i.e. atomic forces) to determine the direction of structural change [46]. In contrast to simple gradient-descent methods, such algorithms use information from previous iterations to accelerate convergence.

As a result of geometry optimisation, the initial structural candidates are transformed into energetically stable relaxed structures. The resulting equilibrium geometry serves as the basis for subsequent calculations of vibrational, electronic, and optical properties of the material.

3.5 Properties calculations

Calculation of vibrational, electronic and optical properties of the optimised compound provides information about the dynamical stability, electronic structure, and optical response to electromagnetic radiation.

3.5.1 Vibrational properties

The first step after the structural optimisation is the analysis of the phonon spectrum, since the dynamical stability of a crystal is determined by its lattice vibrations [47]. In crystals, due to the thermal motion, atoms oscillate around their equilibrium positions. These collective vibrational excitations are called phonons. A dynamically stable structure corresponds not only to a local energy minimum obtained during geometry optimisation, but is also characterised by the absence of imaginary phonon modes throughout the first Brillouin zone. The first Brillouin zone is the primitive cell of the reciprocal lattice and describes the wave-vector space of the crystal [16].

In the harmonic approximation, lattice vibrations are described by the dynamical matrix. The corresponding eigenvalue problem can be written as

$$De = \omega^2 e, \tag{5}$$

where D is the dynamical matrix, ω denotes the phonon frequencies, and e represents the vibrational eigenvectors. Positive values of ω^2 correspond to stable vibrational modes, whereas negative values lead to imaginary frequencies. Phonon dispersion relations are typically calculated along high-symmetry paths in the first Brillouin zone. For the cubic space group $F\bar{4}3m$ (No. 216), the corresponding high-symmetry k-points and Brillouin-zone path can be obtained from Ref. [48].

Phonon spectra in DFT can be obtained using either the finite-displacement method or density functional perturbation theory (DFPT) [49]. In the present work, the finite-displacement approach was employed.

In the finite-displacement approach, atoms are displaced slightly from their equilibrium positions. The atomic displacements must remain sufficiently small in order to minimise anharmonic contributions. The resulting forces are calculated using DFT. These forces are then used to construct the force-constant matrix and the dynamical matrix of the crystal, from which the phonon frequencies and vibrational modes are obtained.

For a crystal containing N atoms in the primitive cell, the phonon spectrum consists of $3N$ vibrational branches. Three of these branches correspond to acoustic modes associated with translational

motion of the lattice, while the remaining modes are optical phonons. At the Γ-point (centre of the Brillouin zone), the acoustic phonon frequencies approach zero due to the translational invariance of the crystal.

3.5.2 Electronic properties

Electronic-structure calculations are performed for the optimised crystal structures in order to analyse the density of states (DOS) and band-gap properties. The electronic SCF procedure used in static electronic-structure calculations is identical to that employed during geometry optimisation. However, in static calculations ionic relaxation is not performed, hence the atomic positions and lattice parameters remain fixed, and only the electronic subsystem is iterated until convergence. Such calculations are commonly referred to as static single-point calculations.

The DOS describes the distribution of electronic states over energy [50] and provides information about occupied and unoccupied electronic states, which allows determination of the electronic band gap (E_g) separating the valence and conduction bands. The size of the band gap can be used to determine whether a material behaves as a metal ($E_g \approx$ 0 eV), semiconductor ($E_g \approx$ 0.1–3 eV), or insulator ($E_g \gtrsim$ 3 eV), and to estimate the energy range of optical transitions. In addition to the total DOS, projected density of states (PDOS) calculations show the contributions of specific atoms and atomic orbitals to the electronic structure of the material.

Electronic-structure calculations can be initially performed using PBE [31]. However, semi-local approximations frequently underestimate electronic band gaps. To improve the description of electronic states and band-gap values, hybrid functionals [35] are employed. For DOS calculations carried out in this work, Brillouin-zone integrations were performed using the tetrahedron method [51].

3.5.3 Optical properties

The interaction of a crystal with electromagnetic radiation is described by its optical properties. Optical processes in crystals are associated with electronic transitions between occupied and unoccupied electronic states caused by incident light (electromagnetic radiation) [52]. Therefore, the optical response of a material is directly related to the electronic structure and E_g.

The optical response of a material can be described by the complex dielectric function

$$\varepsilon(\omega) = \varepsilon_1(\omega) + i\varepsilon_2(\omega), \tag{6}$$

where $\varepsilon_1(\omega)$ is the real part of the dielectric function and $\varepsilon_2(\omega)$ is the imaginary part. The imaginary part describes optical absorption caused by interband electronic transitions, whereas the real part describes the polarisation of the material in an external electromagnetic field.

The dielectric function is related to experimentally measurable optical quantities such as the

absorption coefficient, refractive index, and reflectivity, which are important for the analysis of photochromic materials.

Once the dielectric function is obtained, the absorption coefficient can be calculated as

$$\alpha(\omega) = \frac{\sqrt{2}\,\omega}{c}\left(\sqrt{\varepsilon_1^2(\omega) + \varepsilon_2^2(\omega)} - \varepsilon_1(\omega)\right)^{1/2}, \tag{7}$$

where c is the speed of light and ω is the angular frequency of the electromagnetic wave. The absorption coefficient describes how strongly electromagnetic radiation is absorbed inside the material as a function of photon energy $\hbar\omega$.

4 Results

The YHO structure was constructed and subsequently analysed in *VASP* using a sequence of DFT calculations including geometry optimisation, phonon, electronic density of states (DOS), and optical-property calculations. The INCAR and KPOINTS files used in the calculations are presented in Appendices C and D. Parameters specific to individual calculations are described in the corresponding sections.

4.1 Crystal structure construction

The initial crystal structure used for the construction of yttrium oxyhydride was fluorite-type yttrium dihydride YH_2, crystallising in the cubic space group $Fm\bar{3}m$ (No. 225). The conventional unit cell of YH_2 contains four yttrium atoms and eight hydrogen atoms (Y_4H_8). In the parent structure, yttrium atoms occupy the $4a$ Wyckoff positions at $(0, 0, 0)$, forming a fcc sublattice, while hydrogen atoms occupy the tetrahedral interstitial $8c$ positions at $(1/4, 1/4, 1/4)$.

Table 3: Wyckoff positions of the parent fluorite-type YH_2 structure ($Fm\bar{3}m$, No. 225).

Atom	Wyckoff position	Multiplicity	Coordinates
Y	4a	4	$(0, 0, 0)$
H	8c	8	$(1/4, 1/4, 1/4)$

The YHO structure was generated by ordered substitution of half of the hydrogen atoms with oxygen atoms in order to obtain the Y : H : O = 1 : 1 : 1 stoichiometry corresponding to the conventional composition $Y_4H_4O_4$. In the initial $Fm\bar{3}m$ structure, all hydrogen atoms occupying the $8c$ positions are symmetry-equivalent. After ordered substitution, the equivalence of these tetrahedral positions is broken, resulting in splitting of the original $8c$ Wyckoff position into two independent sublattices:

$$8c \rightarrow 4a + 4b. \tag{8}$$

Table 4: Wyckoff positions of the ordered YHO structure ($F\bar{4}3m$, No. 216) obtained after symmetry lowering.

Atom	Wyckoff position	Multiplicity	Coordinates
Y	4c	4	$(1/4, 1/4, 1/4)$
H	4a	4	$(0, 0, 0)$
O	4b	4	$(1/2, 1/2, 1/2)$

As a consequence, the symmetry of the crystal structure is reduced from $Fm\bar{3}m$ to the cubic subgroup $F\bar{4}3m$ (No. 216), obtained from subgroup analysis using the Bilbao Crystallographic

Server [5, 12].

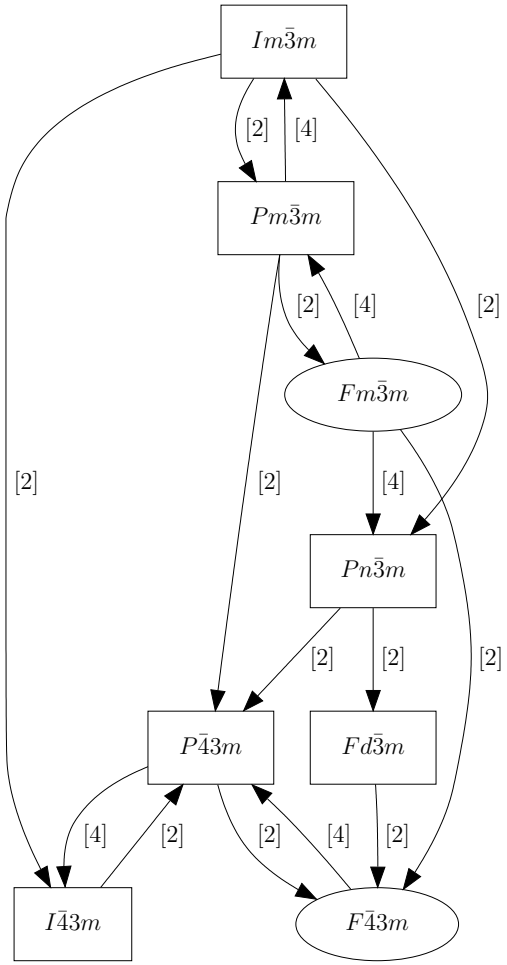

Figure 1: Group-subbgroup relation between the parent $Fm\bar{3}m$ and the ordered $F\bar{4}3m$ structures generated using the Bilbao Crystallographic Server [5, 12].

In the resulting ordered structure, yttrium atoms occupy the $4c$ positions at $(1/4, 1/4, 1/4)$, hydrogen atoms occupy the $4a$ positions at $(0, 0, 0)$, and oxygen atoms occupy the $4b$ positions at $(1/2, 1/2, 1/2)$. The resulting structure therefore corresponds to a bipartite ordering of tetrahedral interstitial sites within the fluorite-derived lattice.

The conventional lattice vectors were constructed using the experimental lattice parameter of yttrium dihydride, $a = 5.2$ Å [21], which gives

$$\begin{aligned} \vec{A}_1 &= (5.2, 0.0, 0.0), \\ \vec{A}_2 &= (0.0, 5.2, 0.0), \\ \vec{A}_3 &= (0.0, 0.0, 5.2). \end{aligned} \tag{9}$$

The resulting conventional $Y_4H_4O_4$ unit cell contains the following atomic coordinates:

Table 5: Atomic coordinates of the conventional $Y_4H_4O_4$ unit cell.

Atom	x	y	z
Y	0.25	0.25	0.25
Y	0.25	0.75	0.75
Y	0.75	0.25	0.75
Y	0.75	0.75	0.25
H	0.00	0.00	0.00
H	0.00	0.50	0.50
H	0.50	0.00	0.50
H	0.50	0.50	0.00
O	0.50	0.50	0.50
O	0.50	0.00	0.00
O	0.00	0.50	0.00
O	0.00	0.00	0.50

The corresponding primitive unit cell contains one yttrium, one hydrogen, and one oxygen atom. The primitve lattice vectors are given by:

$$\begin{aligned} \vec{a}_1 &= (0.0, 2.6, 2.6), \\ \vec{a}_2 &= (2.6, 0.0, 2.6), \\ \vec{a}_3 &= (2.6, 2.6, 0.0). \end{aligned} \tag{10}$$

with fractional atomic coordinates given in Table 6.

Table 6: Fractional atomic coordinates of the primitive YHO unit cell.

Atom	x	y	z
Y	0.25	0.25	0.25
H	0.00	0.00	0.00
O	0.50	0.50	0.50

POSCAR file of the constructed structure is presented in Appendix B.1.

4.2 Geometry optimisation

The studied structure, yttrium oxyhydride (YHO), corresponds to the cubic space group $F\bar{4}3m$ (No. 216). The calculations were performed using the primitive rhombohedral representation of the fcc lattice. In this representation, the primitive cell is characterised by lattice angles of 60° and a reduced lattice parameter compared to the conventional cubic cell.

Experimental studies report a conventional cubic lattice parameter of approximately 5.32 Å for YHO (No. 216) [23]. For the primitive fcc representation used in the present work, this corresponds to a lattice parameter of approximately 3.76 Å, according to the relation:

$$a_{\text{prim}} = \frac{a_{\text{conv}}}{\sqrt{2}}. \tag{11}$$

The initial and optimised primitive-cell lattice parameters are compared with the experimental primitive-cell equivalent in Table 7.

The geometry optimisation was performed using the PBE functional. Atomic positions and lattice parameters were relaxed (`ISIF = 3`) until the forces on each atom were below 0.001 eV/Å (`EDIFFG = -0.001`) and the electronic self-consistency reached 10^{-7} eV (`EDIFF = 1E-7`). A plane-wave energy cutoff of 700 eV (`ENCUT = 700`) and a dense Fast Fourier Transform (FFT) grid (`PREC = Accurate`, `ADDGRID = .TRUE.`) were used to reduce numerical noise in the calculations.

K-point sampling was performed using a Γ-centred Monkhorst-Pack grid. Convergence with respect to k-point density was tested by comparing total energies obtained with different meshes. For $4 \times 4 \times 4$ and $5 \times 5 \times 5$ grids, the total energies are -21.67452 eV and -21.67466 eV, respectively. The difference of 1.4×10^{-4} eV indicates that a $4 \times 4 \times 4$ mesh is sufficient for convergence. A denser $6 \times 6 \times 6$ grid was used in subsequent calculations to ensure higher accuracy.

The geometry optimisation converged for both electronic and ionic steps. The final total energy of the system is -21.680 eV, indicating a stable local minimum.

The structural changes after the optimisation are negligible. The lattice parameters $a = b = c$ increased from 3.677 Å to 3.743 Å ($\approx 1.8\%$), indicating that the initial structure was already close to equilibrium. The optimised lattice parameter is also in good agreement with the experimental value of 3.76 Å. At convergence, residual forces are close to zero, the residual pressure is 0.091 kB.

The optimised structure file, CONTCAR, was subsequently used as the POSCAR input for all following calculations.

Table 7: Lattice parameters of the YHO structure before and after optimisation.

State	a (Å)	b (Å)	c (Å)	α (°)	β (°)	γ (°)
Initial	3.677	3.677	3.677	60	60	60
Optimised	3.743	3.743	3.743	60	60	60
Experimental [23]	3.76	3.76	3.76	60	60	60

Table 8: Atomic positions in fractional coordinates.

Atom	x	y	z	Wyckoff
Y	0.25	0.25	0.25	4c
O	0.00	0.00	0.00	4a
H	0.50	0.50	0.50	4b

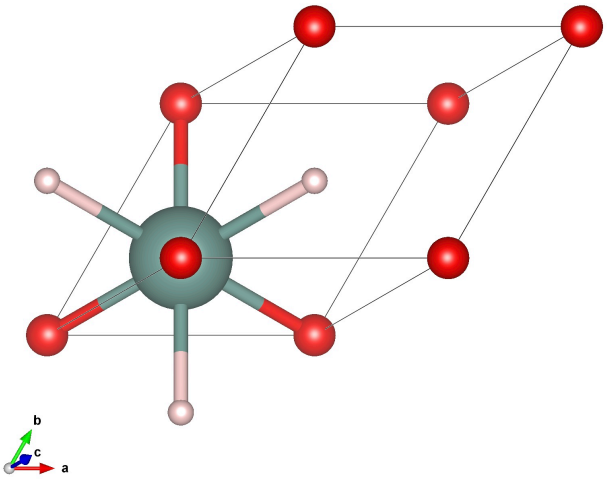

Figure 2: Optimised crystal structure of YHO in the $F\bar{4}3m$ space group. Y atom is shown in light green, O atoms in red, and H in light pink.

4.3 Vibrational properties

Phonon dispersion relations (phonon band structure) were calculated using the finite-displacement method implemented in *phonopy* [41]. Using the optimised structure, $2 \times 2 \times 2$ supercells were created and symmetrically inequivalent atomic displacements (`disp-001`, `disp-002`, `disp-003`) were generated.

For each displaced supercell, single-point calculations were performed using the PBE functional in *VASP* to obtain the atomic forces. A Γ-centred $3 \times 3 \times 3$ k-point mesh was used for the supercell calculations, corresponding to the $6 \times 6 \times 6$ mesh used for the primitive cell. The electronic convergence criterion was set to 10^{-8} eV. Symmetry was disabled (`ISYM = 0`) in order to avoid symmetrisation of the displaced atomic configurations. Gaussian smearing (`ISMEAR = 0`, `SIGMA = 0.05`) was used to reduce numerical noise in the calculated energy and forces.

The force constants were then extracted from the computed forces and used to evaluate the phonon band structure. The phonon dispersion curves were calculated along high-symmetry paths in the Brillouin zone, automatically determined using SeeK-path [53].

All calculated phonon frequencies (Fig. 3) remain positive throughout the Brillouin zone. This confirms that the structure is dynamically stable. The three acoustic branches approach zero at the Γ-

point. The highest phonon frequencies reach 33.8 THz. Low-frequency modes are mainly associated with the motion of heavy Y atoms, whereas high-frequency peaks originate from vibrations of light H atoms.

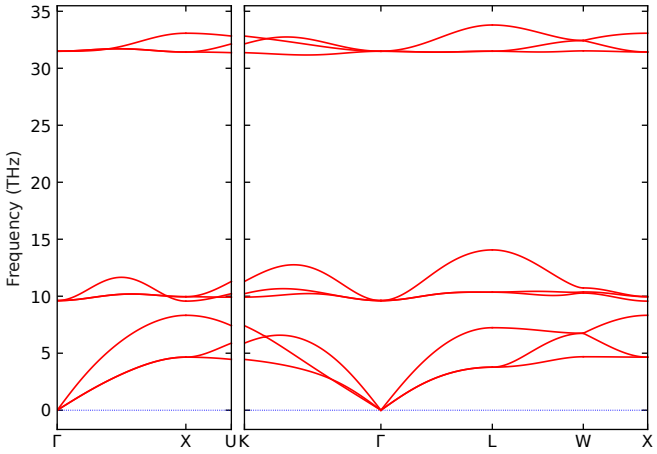

Figure 3: Phonon dispersion relations calculated for the optimized YHO structure.

4.4 Electronic properties

Electronic density of states was calculated sequentially using two functionals: PBE and HSE06. Static single-point calculations were performed without ionic relaxation (`NSW = 0`). The tetrahedron method (`ISMEAR = -5` with `NEDOS = 2000`) was used to improve resolution of DOS peaks and band edges. Projected density of states (PDOS) calculations were performed using `LORBIT = 11`. Since GGA functionals have a tendency to underestimate band gaps, HSE06 was used to perform second-step DOS calculations. The converged CHGCAR and WAVECAR files (charge density and wavefunctions, respectively) from the PBE calculations were used as the initial guess HSE06 calculations.

As shown in Fig. 4, the PBE calculations predict a clear band gap at Fermi energy level of 3.96 eV, indicating insulating behaviour. The HSE06 calculations shown in Fig. 5 increased band gap to 5.31 eV.

The overall shape of the DOS remains similar for both functionals, but the conduction-band states are shifted to higher energies in the HSE06 calculations. The valence band is dominated mainly by O $2p$ states with smaller contributions from H orbitals, whereas the conduction band is formed predominantly by Y d states.

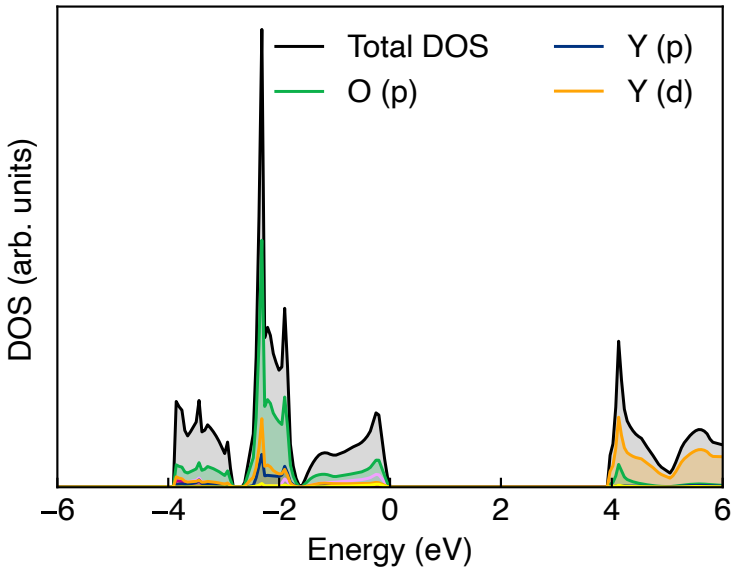

Figure 4: Total (TDOS) and projected (PDOS) density of states calculated using the PBE functional.

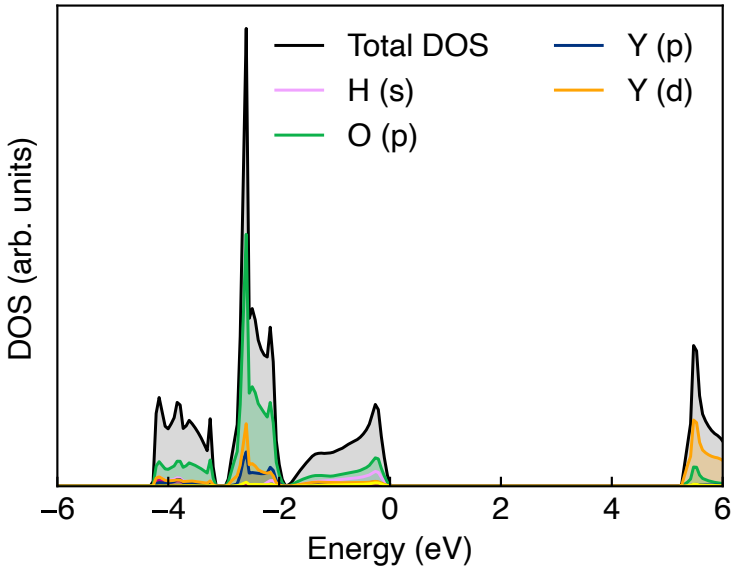

Figure 5: Total (TDOS) and projected (PDOS) density of states calculated using the HSE06 functional.

Table 9: Calculated electronic band gaps (E_g) of YHO.

Functional	Band gap (eV)
PBE	3.96
HSE06	5.31

4.5 Optical properties

Optical properties were calculated using the HSE06 functional with `LOPTICS = .TRUE.` (which calculates the frequency dependent dielectric matrix). Since optical calculations require a sufficient number of unoccupied conduction-band states, the number of bands was increased from the *VASP* default value of 16 to 48 for all preceding electronic-structure and optical calculations [54]. This improves the description of interband electronic transitions contributing to the dielectric function and optical absorption spectra. The converged CHGCAR and WAVECAR files obtained from the preceding HSE06 DOS calculations were used as the initial guess for the optical calculations. Gaussian smearing (`ISMEAR = 0`, `SIGMA = 0.05`) was used. The final optical calculations were performed using a denser 10 $\times$ 10 $\times$ 10 k-point mesh after convergence testing, since it produced smoother optical spectra compared to the 6 $\times$ 6 $\times$ 6 mesh.

The calculated real part of the dielectric function is shown in Fig. 6. At low photon energies, ε_1 is positive, with a dimensionless value of about 4, which describes the low-energy electronic response of the material to the electromagnetic field. As the photon energy increases, ε_1 rises rapidly and reaches its maximum close to 10 eV. Therefore, it can be stated that YHO has the strongest electronic transitions at this energy region. After the main maximum, ε_1 decreases sharply. A weaker peak is then observed at higher energies. In the whole range, ε_1 remains positive, which means that the material does not show metallic behaviour.

The imaginary part of dielectric function, ε_2 (shown in Fig. 7), represents the absorptive part of the dielectric response. At low photon energies its value is close to zero, as expected for an insulator with a pronounced band gap. The first and strongest peak appears near 10 eV, as also observed for ε_1. This peak corresponds to interband transitions from occupied valence states to empty conduction-band states above the band gap. A second, weaker peak appears at about 40 eV, which can be assigned to higher-energy electronic excitations. Afterwards, ε_2 rapidly tends to zero, indicating weaking optical transitions at highest energies.

The pronounced peaks of the dielectric function are associated with regions of high electronic density of states and enhanced probabilities of interband transitions. The main optical transitions are related to excitations from valence states (predominantly O- and H-derived states) to conduction-band states (Y-derived states), which is consistent with the calculated DOS results (see Fig. 5).

The calculated absorption spectrum is shown in Fig. 8. The absorption coefficient is zero at low photon energies (up to 4 eV) and increases significantly in the deep-ultraviolet region, consistent with the large HSE06 band gap obtained from the DOS calculations. The optical response is therefore dominated by high-energy interband electronic transitions. A comparison with the experimental absorption spectrum is shown in Fig. 9.

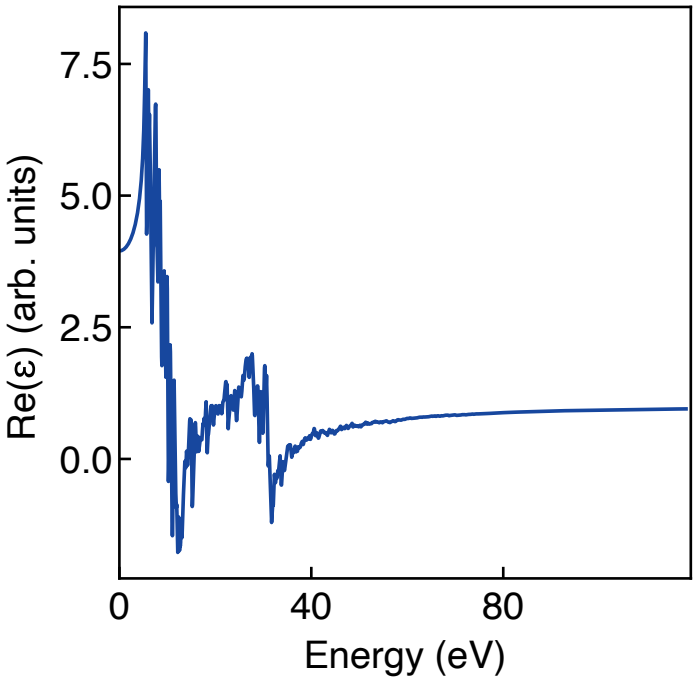

Figure 6: Real part of the frequency-dependent dielectric function of YHO.

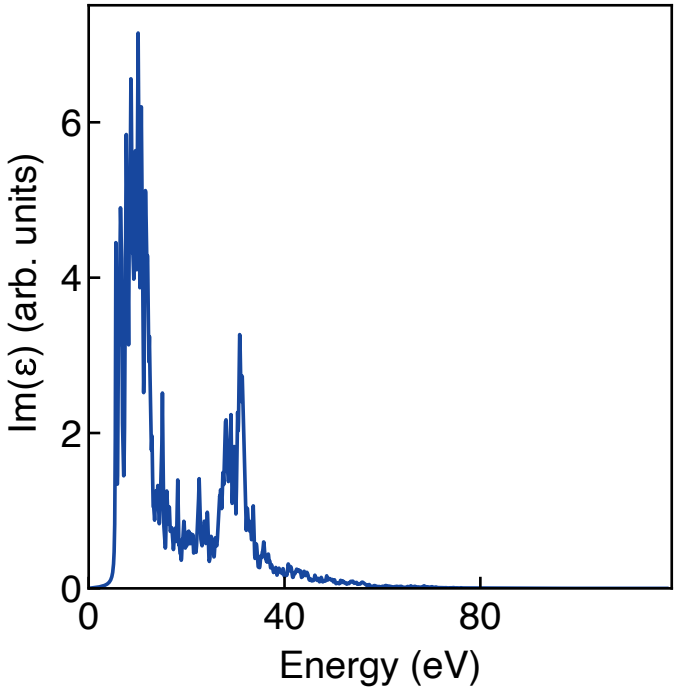

Figure 7: Imaginary part of the frequency-dependent dielectric function of YHO.

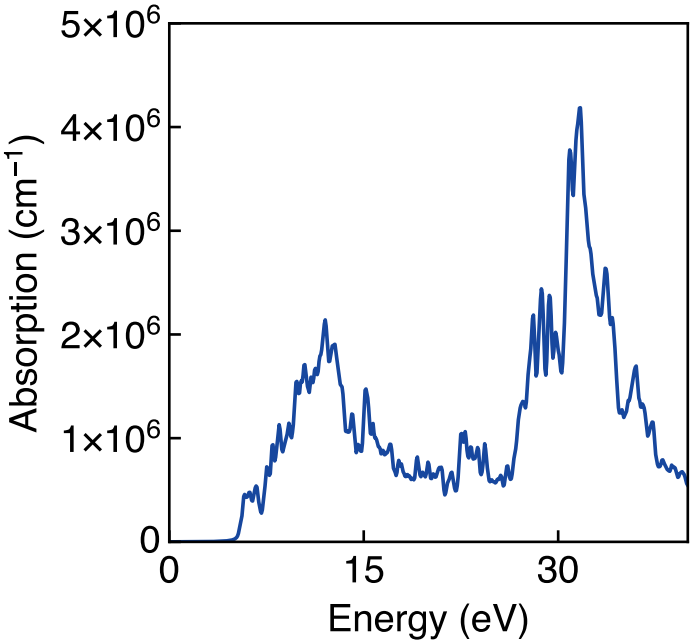

Figure 8: Calculated optical absorption spectrum of YHO.

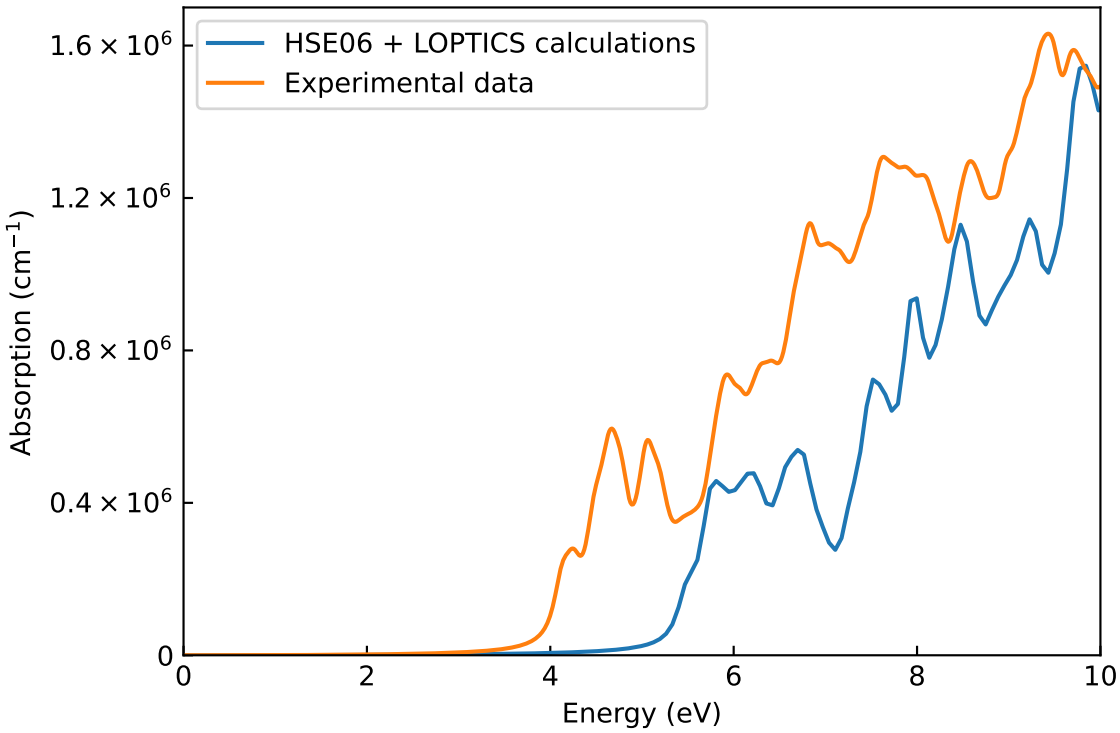

Figure 9: Comparison of the calculated HSE06 optical absorption spectrum with experimental data from Ref. [55] near the boundary of absorption.

5 Discussion

The crystal structure of YHO has not yet been determined unambiguously. X-ray diffraction (XRD) measurements do not allow a unique identification of the crystal symmetry due to possible structural disorder, coexistence of multiple phases, and the weak X-ray scattering of hydrogen atoms. The calculations presented in this work were performed for one of the possible crystal structures obtained using a symmetry-based approach and may contribute to the identification of the most probable crystal structure.

The calculated phonon spectrum (Fig. 3) is divided into several clearly separated frequency regions, which is expected for YHO [56]. The high-frequency region is dominated mainly by vibrations of hydrogen atoms, the intermediate-frequency region by oxygen vibrations, and the low-frequency region is dominated primarily by yttrium atoms. This separation is related to the significant differences in the atomic masses of the component elements.

All calculated phonon frequencies are real and no imaginary phonon modes are present, which means that the structure is dynamically stable with respect to small atomic displacements from the equilibrium positions. This result allows to further investigate the electronic and optical properties of YHO.

The PBE and HSE06 calculations give significantly different values of the band gap E_g (Table 9). The reason for that is that standard GGA functionals typically underestimate the band gap. Therefore, the subsequent optical-property calculations were performed using the hybrid HSE06 functional, which combines exact Hartree-Fock exchange with the DFT approach and provides a more realistic description of the electronic structure.

The band gap, calculated with HSE06, is close to the experimental value [22], consistent with the dielectric character of the material. The obtained E_g value corresponds to the far-ultraviolet (UVC) spectral region with a wavelength of 233.5 nm.

The overlap of s-, p-, and d-orbital contributions in the PDOS (Fig. 5) indicates mixing (hybridisation) of the electronic states. However, the relatively large interatomic distances (for example, O-H 2.65 Å) suggest that the crystal is weakly covalent and that the chemical bonding has a predominantly ionic-covalent character with a relatively small covalent contribution. The large band gap is also consistent with a high localisation of the valence electronic states, indicating a significant ionic contribution to the chemical bonding.

The calculated absorption spectrum shows good agreement with the experimental data (Fig. 9) [55]. However, a shift of the absorption edge of approximately 2 eV is observed between the two curves. This difference may be related to excitonic effects [57], observed in the experimental spectrum near 4–6 eV, which are not captured within the HSE06 approach.

Further research in this field is related to the investigation of a broader class of rare-earth and transition-metal oxyhydrides (XOH, X = Sc, Nd, Sm, Gd, Er, Dy, La, Ce, Pr, Tb, Ho, Er, Lu [58]). Multicomponent oxyhydride structures are also of particular interest, since they may allow the

combination of properties of different compounds as well as the stabilisation of metastable phases through partial substitution. Such materials are considered promising candidates for the development of new functional materials.

The mechanism of the photochromic effect in yttrium oxyhydrides remains an open question. At present, three main mechanisms are discussed in the literature. The first is associated with the formation of strong excitonic peaks near the conduction-band minimum, which effectively reduce the band gap [57]. The second proposes local distortions of the crystal lattice caused by hydrogen displacement due to strong electron-phonon interactions [59]. The third mechanism is related to the formation of hydrogen or oxygen vacancies and, consequently, the appearance of additional electronic states inside the band gap that may modify the electronic and optical properties of the material [60]. All three proposed mechanisms require further investigation.

Using the described methodology, calculations were also performed for a class of crystals with potential photochromic properties belonging to the space group $F\bar{4}3m$, including LaHO, NbHO, NdHO, and ZrHO, provided in Appendix E.

6 Conclusions

In this work, the crystal structure and physical properties of yttrium oxyhydride (YHO) were investigated using first-principles density functional theory calculations implemented in *VASP*.

A symmetry-based approach was used to construct the YHO crystal structure starting from the fluorite-type yttrium dihydride parent phase. Ordered substitution of hydrogen by oxygen atoms resulted in symmetry lowering from the cubic space group $Fm\bar{3}m$ (No. 225) to the ordered $F\bar{4}3m$ (No. 216) structure.

Geometry optimisation using the PBE functional demonstrated that the optimised lattice parameters are in good agreement with experimental data. The calculated phonon dispersion relations contain no imaginary frequencies, confirming the dynamical stability of the obtained structure.

Electronic-structure calculations showed insulating behaviour of YHO. The calculated band gap increased from 3.96 eV within PBE to 5.31 eV using the HSE06 hybrid functional, showing that hybrid functionals provide a more realistic description of the electronic structure of YHO.

Optical calculations based on the HSE06 functional were used to obtain the dielectric function and optical absorption spectrum of YHO. The calculated absorption spectrum showed good agreement with experimental data. A differnece near the absorption edge may be related to excitonic effects not captured within the independent-particle approximation used in the present work.

The results show that the symmetry-based structure construction method followed by first-principles calculations is an effective approach for predicting and investigating mixed-anion structures such as oxyhydrides.

Acknowledgements

I am deeply grateful to my supervisors, Dr. Mihhail Klopov and Dr. Smagul Karazhanov, for their continuous guidance, for helping me develop the theoretical and practical understanding required for this work, for their time, and for sharing their enthusiasm for the topic.

I would also like to thank Dr. Evgenii Strugovshchikov for an important contribution to this thesis, for patience, and for detailed and systematic explanations of new and challenging topics.

The author and supervisors acknowledge the LZP-2024/1-0632 project “Innovative Thin Films of Rare-Earth Metal Oxyhydrides: Unlocking New Applications” funded by Latvian Science Council.

References

[1] Z. L. Wang and Z. C. Kang, *Functional and Smart Materials: Structural Evolution and Structure Analysis*, Springer, 1998. doi: 10.1007/978-1-4615-5367-0.

[2] T. Mongstad, C. Platzer-Björkman, J. P. Maehlen, L. P. A. Mooij, Y. Pivak, B. Dam, E. S. Marstein, B. C. Hauback, and S. Zh. Karazhanov, "A new thin film photochromic material: Oxygen-containing yttrium hydride," *Solar Energy Materials and Solar Cells*, vol. 95, no. 12,pp. 3596–3599, 2011. doi: 10.1016/j.solmat.2011.08.018.

[3] P. Hohenberg and W. Kohn, "Inhomogeneous Electron Gas," *Physical Review*, vol. 136, no. 3B, pp. B864–B871, 1964. doi: 10.1103/PhysRev.136.B864.

[4] W. Kohn and L. J. Sham, "Self-Consistent Equations Including Exchange and Correlation Effects," *Physical Review*, vol. 140, no. 4A, pp. A1133–A1138, 1965. doi: 10.1103/PhysRev.140.A1133.

[5] M. I. Aroyo, J. M. Perez-Mato, C. Capillas, E. Kroumova, S. Ivantchev, G. Madariaga, A. Kirov, and H. Wondratschek, "Bilbao Crystallographic Server: I. Databases and crystallographic computing programs," *Zeitschrift für Kristallographie - Crystalline Materials*, vol. 221, pp. 15–27, 2006. doi: 10.1524/zkri.2006.221.1.15.

[6] D. Frenkel and B. Smith, *Understanding Molecular Simulation: From Algorithms to Applications* 2nd ed. Academic Press, 2001. doi: 10.1016/B978-0-12-267351-1.X5000-7.

[7] A. R. Oganov and C. W. Glass, "Crystal structure prediction using ab initio evolutionary techniques: Principles and applications," *The Journal of Chemical Physics*, vol. 124, p. 244704, 2006. doi: 10.1063/1.2210932.

[8] K. T. Butler, D. W. Davies, H. Cartwright, O. Isayev, and A. Walsh, "Machine learning for molecular and materials science," *Nature*, vol. 559, pp. 547–555, 2018. doi: 10.1038/s41586-018-0337-2.

[9] S. Curtarolo, W. Setyawan, G. L. W. Hart, M. Jahnatek, R. V. Chepulskii, R. H. Taylor, S. Wang, J. Xue, K. Yang, O. Levy, M. J. Mehl, H. T. Stokes, D. O. Demchenko, and D. Morgan, "AFLOW: An automatic framework for high-throughput materials discovery," *Computational Materials Science*, vol. 58, pp. 218–226, 2012. doi: 10.1016/j.commatsci.2012.02.005.

[10] D. Hicks, M. J. Mehl, E. Gossett, C. Toher, O. Levy, R. M. Hanson, G. Hart, and S. Curtarolo, "The AFLOW Library of Crystallographic Prototypes: Part 2," *Computational Materials Science*, vol. 161, pp. S1–S1011, 2019. doi: 10.1016/j.commatsci.2018.10.043.

[11] H. Eckert, S. Divilov, M. J. Mehl, D. Hicks, A. C. Zettel, M. Esters, X. Campilongo, and S. Curtarolo, "The AFLOW Library of Crystallographic Prototypes: Part 4," *Computational Materials Science*, vol. 240, p. 112988, 2024. doi: 10.1016/j.commatsci.2024.112988.

[12] M. I. Aroyo, Ed., *International Tables for Crystallography, Volume A: Space-Group Symmetry*, 2nd online ed. Wiley, 2016. doi: 10.1107/97809553602060000114.

[13] G. Kresse and J. Furthmüller, “Efficient iterative schemes for ab initio total-energy calculations using a plane-wave basis set,” *Physical Review B*, vol. 54, pp. 11169–11186, 1996. doi: 10.1103/PhysRevB.54.11169.

[14] G. Kresse and J. Furthmüller, “Efficiency of ab-initio total energy calculations for metals and semiconductors using a plane-wave basis set,” *Computational materials science*, vol. 6, pp. 15–50, 1996. doi: 10.1016/0927-0256(96)00008-0.

[15] N. W. Ashcroft and N. D. Mermin, *Solid State Physics*. Holt, Rinehart and Winston, 1976.

[16] C. Kittel, *Introduction to Solid State Physics*, 8th ed. Wiley, 2004.

[17] F. Nafezarefi, *Photochromic Properties of Rare-Earth Oxyhydrides*, Ph.D. dissertation, Delft University of Technology, Delft, Netherlands, 2020. doi: 10.4233/uuid:eb54d12f-079a-41a4-8d75-1a0fdf2af412.

[18] H. Kageyama, K. Hayashi, K. Maeda, J. P. Attfield, Z. Hiroi, J. M. Rondinelli, and K. R. Poeppelmeier, “Expanding frontiers in materials chemistry and physics with multiple anions,” *Nature Communications*, vol. 9, no. 1, p. 772, 2018. doi: 10.1038/s41467-018-02838-4.

[19] A. Pishtshev, E. Strugovshchikov, and S. Karazhanov, “Conceptual design of yttrium oxyhydrides: phase diagram, structure, and properties,” *Crystal Growth & Design*, vol. 19, no. 5, pp. 2574–2582, 2019. doi: 10.1021/acs.cgd.8b01596.

[20] E. Strugovshchikov, A. Pishtshev, and S. Karazhanov, “Orthogonal chemistry in the design of rare-earth metal oxyhydrides,” *Pure and Applied Chemistry*, vol. 93, no. 11, pp. 1293–1299, 2021. doi: 10.1515/pac-2021-0207.

[21] J. Montero, F. A. Martinsen, M. Lelis, S. Zh. Karazhanov, B. C. Hauback, and E. S. Marstein, “Preparation of yttrium hydride-based photochromic films by reactive magnetron sputtering,” *Solar Energy Materials and Solar Cells*, vol. 177, pp. 106–109, 2018. doi: 10.1016/j.solmat.2017.02.001.

[22] S. Cornelius, G. Colombi, F. Nafezarefi, H.Schreuders, R. Heller, F. Munnik, and B. Dam, “Oxyhydride nature of rare-earth-based photochromic thin films,” *The Journal of Physical Chemistry Letters*, vol. 10, no. 12, pp. 1342–1348, 2019. doi: 10.1021/acs.jpclett.9b00088.

[23] M. H. Sørby, F. Martinsen, S. Zh. Karazhanov, B. C. Hauback, and E. S. Marstein, “On the crystal chemistry of photochromic yttrium oxyhydride,” *Energies*, vol. 15, no. 5, art. no. 1903, 2022. doi: 10.3390/en15051903.

[24] Y. Wang, J. Lv, L. Zhu, and Y. Ma, “CALYPSO: A method for crystal structure prediction,” *Computer Physics Communications*, vol. 183, no. 10, pp. 2063–2070, 2012. doi: 10.1016/j.cpc.2012.05.008.

[25] C. J. Pickard and R. J. Needs, “Ab initio random structure searching,” *Journal of Physics: Condensed Matter*, vol. 23, no. 5, p. 053201, 2011. doi: 10.1088/0953-8984/23/5/053201.

[26] D. M. Ceperley and B. J. Alder, “Ground state of the electron gas by a stochastic method,” *Physical Review Letters*, vol. 45, pp. 566–569, 1980. doi: 10.1103/PhysRevLett.45.566.

[27] J. P. Perdew and A. Zunger, “Self-interaction correction to density-functional approximations for many-electron systems,” *Physical Review B*, vol. 23, no. 10, pp. 5048–5079, 1981. doi: 10.1103/PhysRevB.23.5048.

[28] J. P. Perdew, J. A. Chevary, S. H. Vosko, K. A. Jackson, M. R. Pederson, D. J. Singh, and C. Fiolhais, “Atoms, molecules, solids, and surfaces: Applications of the generalized gradient approximation for exchange and correlation,” *Physical Review B*, vol. 46, no. 11, pp. 6671–6687, 1992. doi: 10.1103/PhysRevB.46.6671.

[29] S. Grimme, “Semiempirical hybrid density functional with perturbative second-order correlation,” *The Journal of Chemical Physics*, vol. 124, no. 3, 2006. doi: 10.1063/1.2148954.

[30] M. Marsman, A. Grüneis, J. Paier, and G. Kresse, “Second-order Møller–Plesset perturbation theory applied to extended systems. I. Within the projector-augmented-wave formalism using a plane wave basis set,” *The Journal of Chemical Physics*, vol. 130, no. 18, p. 184103, 2009. doi: 10.1063/1.3126249.

[31] J. P. Perdew, K. Burke, and M. Ernzerhof, “Generalized Gradient Approximation Made Simple,” *Physical Review Letters*, vol. 77, no. 18, pp. 3865–3868, 1996. doi: 10.1103/PhysRevLett.77.3865.

[32] P. E. Blöchl, “Projector augmented-wave method,” *Physical Review B*, vol. 50, no. 24, pp. 17953–17979, 1994. doi: 10.1103/PhysRevB.50.17953.

[33] G. Kresse and D. Joubert, “From ultrasoft pseudopotentials to the projector augmented-wave method,” *Physical Review B*, vol. 59, no. 3, pp. 1758–1775, 1999. doi: 10.1103/PhysRevB.59.1758.

[34] M. Dion, H. Rydberg, E. Schröder, D. C. Langreth, and B. I. Lundqvist, “Van der Waals density functional for general geometries,” *Physical Review Letters*, vol. 92, no. 24, p. 246401, 2004. doi: 10.1103/PhysRevLett.92.246401.

[35] J. Heyd, G. E. Scuseria, and M. Ernzerhof, “Hybrid functionals based on a screened Coulomb potential,” *The Journal of Chemical Physics*, vol. 118, no. 18, pp. 8207–8215, 2003. doi: 10.1063/1.1564060.

[36] L. Hedin, “New method for calculating the one-particle Green’s function with application to the electron-gas problem,” *Physical Review*, vol. 139, no. 3A, pp. A796–A823, 1965. doi: 10.1103/PhysRev.139.A796.

[37] D. C. Langreth and J. P. Perdew, “The exchange-correlation energy of a metallic surface,” *Solid State Communications*, vol. 17, no. 11, pp. 1425–1429, 1975. doi: 10.1016/0038-1098(75)90618-3.

[38] F. Furche, “Molecular tests of the random phase approximation to the exchange-correlation energy functional,” *Physical Review B*, vol. 64, no. 19, p. 195120, 2001. doi: 10.1103/PhysRevB.64.195120.

[39] A. V. Krukau, O. A. Vydrov, A. F. Izmaylov, and G. E. Scuseria, “Influence of the exchange screening parameter on the performance of screened hybrid functionals,” *The Journal of Chemical Physics*, vol. 125, no. 22, p. 224106, 2006. doi: 10.1063/1.2404663.

[40] K. Momma and F. Izumi, “VESTA 3 for three-dimensional visualization of crystal, volumetric and morphology data,” *Journal of Applied Crystallography*, vol. 44, no. 6, pp. 1272–1276, 2011. doi: 10.1107/S0021889811038970.

[41] A. Togo, L. Chaput, T. Tadano, and I. Tanaka, “Implementation strategies in phonopy and phono3py,” *Journal of Physics: Condensed Matter*, vol. 35, no. 35, p. 353001, 2023. doi: 10.1088/1361-648X/acd831.

[42] A. M. Ganose, A. J. Jackson, and D. O. Scanlon, “sumo: Command-line tools for plotting and analysis of periodic ab initio calculations,” *Journal of Open Source Software*, vol. 3, no. 28, p. 717, 2018. doi: 10.21105/joss.00717.

[43] OpenAI, “ChatGPT,” https://chatgpt.com/, accessed May 2026.

[44] E. G. Lewars, *Computational Chemistry: Introduction to the Theory and Applications of Molecular and Quantum Mechanics*, 2nd ed. Springer, 2011. doi: 10.1007/978-90-481-3862-3.

[45] VASP Wiki, “Structure Optimization.” `https://vasp.at/wiki/Structure_optimization` (Accessed: May 16, 2026).

[46] M. Watkins, “Protocols for Geometry and Cell Optimization,” CECAM Tutorial, 2015. `https://www.cp2k.org/_media/events:2015_cecam_tutorial:watkins_optimization.pdf` (Accessed: May 16, 2026).

[47] A. Togo and I. Tanaka, “First principles phonon calculations in materials science,” *Scripta Materialia*, vol. 108, pp. 1–5, 2015. doi: 10.1016/j.scriptamat.2015.07.021.

[48] Bilbao Crystallographic Server, “k-vector types and Brillouin zones of the space groups: Space group No. 216.” `https://cryst.ehu.es/cgi-bin/cryst/programs/nph-kv-list?gnum=216&fig=f4q3mf&what=data` (Accessed May 18, 2026).

[49] S. Baroni, S. de Gironcoli, A. Dal Corso, and P. Giannozzi, “Phonons and related crystal properties from density-functional perturbation theory,” *Reviews of Modern Physics*, vol. 73, no. 2, pp. 515–562, 2001. doi: 10.1103/RevModPhys.73.515.

[50] M. Y. Toriyama, A. M. Ganose, M. Dylla, S. Anand, J. Park, M. K. Brod, J. M. Munro, K. A. Persson, A. Jain, and G. J. Snyder, “How to analyse a density of states,” *Materials Today Electronics*, vol. 1, art. no. 100002, 2022. doi: 10.1016/j.mtelec.2022.100002.

[51] P. E. Blöchl, O. Jepsen, and O. K. Andersen, “Improved tetrahedron method for Brillouin-zone integrations,” *Physical Review B*, vol. 49, no. 23, pp. 16223, 1994. doi: 10.1103/PhysRevB.49.16223.

[52] M. Gajdoš, K. Hummer, G. Kresse, J. Furthmüller, and F. Bechstedt, “Linear optical properties in the projector-augmented wave methodology,” *Physical Review B*, vol. 73, no. 4, p. 045112, 2006. doi: 10.1103/PhysRevB.73.045112.

[53] Y. Hinuma, G. Pizzi, Y. Kumagai, F. Oba, and I. Tanaka, "Band structure diagram paths based on crystallography," *Computational Materials Science*, vol. 128, pp. 140–184, 2017. doi: 10.1016/j.commatsci.2016.10.015.

[54] VASP WIKI, "LOPTICS." `https://www.vasp.at/wiki/LOPTICS` (Accessed April 8, 2026).

[55] H. Arslan, A. Kuzmin, V. Kumar Kasi, I. Aulika, D. Moldarev, D. Primetzhofer, M. Wolff, I. Pudza, Ø. Nordseth, and S. Karazhanov, "Anion vacancy-induced photochromism and lattice relaxation in yttrium oxyhydride," *Communications Materials*, vol. 6, art. no. 154, 2025. doi: 10.1038/s43246-025-00868-2.

[56] M. Zubkins, J. Gabrusenoks, R. Aleksis, G. Chikvaidze, E. Strods, V. Vibornijs, A. Lends, K. Kundzins, and J. Purans, "Vibrational properties of photochromic yttrium oxyhydride and oxydeuteride thin films," *Journal of Alloys and Compounds*, vol. 1015, p. 178917, 2025. doi: 10.1016/j.jallcom.2025.178917.

[57] A. Liivand, M. Klopov, and S. Zh. Karazhanov, "Strong Exciton Effects in Yttrium Oxyhydrides: Evaluation in G_0W_0–BSE Approximation," *SSRN*, 2024. doi: 10.2139/ssrn.4858026.

[58] J. Montero-Amenedo, "Photochromism in rare earth oxyhydrides for large-area transmittance control," *Solar Energy Materials and Solar Cells*, vol. 272, p. 112900, 2024. doi: 10.1016/j.solmat.2024.112900.

[59] E. M. Baba, J. Montero, E. Strugovshchikov, E. Ö. Zayim, and S. Karazhanov, "Light-induced breathing in photochromic yttrium oxyhydrides," *Physical Review Materials*, vol. 4, no. 2, p. 025201, 2020. doi: 10.1103/PhysRevMaterials.4.025201.

[60] A. J. E. Rowberg and C. G. Van de Walle, "Defect Properties, Anion Ordering, and Photochromic Mechanism in Yttrium Oxyhydride," *The Journal of Physical Chemistry C*, vol. 128, no. 47, pp. 20387–20395, 2024. doi: 10.1021/acs.jpcc.4c04988.

Abstract

This thesis focuses on the construction and optimisation of yttrium oxyhydride (YHO) and on the calculation of its vibrational, electronic and optical properties, applying first-principles methods. The structure was generated using a symmetry-based approach starting from the yttrium hydride parent structure and subsequently optimised within density functional theory (DFT) using the *VASP* software package. The obtained lattice parameters are in good agreement with experimental data. Phonon calculations were performed using the finite-displacement method implemented in the *phonopy* package in order to investigate the dynamical stability of the structure. Electronic density of states (DOS) and optical-property calculations were subsequently carried out to analyse the physical properties of YHO. The calculated phonon dispersion relations contain no imaginary frequencies, confirming that the optimised structure is dynamically stable. Electronic-structure calculations indicate insulating behaviour with a wide band gap. Optical calculations provided the dielectric function and absorption spectrum of YHO. The calculated optical absorption spectrum shows good agreement with available experimental data. The main results include the relaxed crystal geometry, phonon dispersion relations, DOS, and optical spectra of yttrium oxyhydride.

Annotatsioon

Käesolev bakalaureusetöö käsitleb ütriumoksühüdriidi (YHO) konstrueerimist ja optimeerimist ning selle vibratsiooniliste, elektrooniliste ja optiliste omaduste arvutamist esimestest printsiipidest lähtuvate meetodite abil. Struktuur genereeriti sümmeetrial põhineva lähenemise abil, lähtudes ütriumhüdriidi algstruktuurist, ning optimeeriti seejärel tihedusfunktsionaali teooria (DFT) raames, kasutades tarkvarapaketti *VASP*. Saadud võreparameetrid on kooskõlas eksperimentaalandmetega. Foononite arvutused viidi läbi lõplike nihete meetodiga, mis on realiseeritud paketis *phonopy*, et uurida struktuuri dünaamilist stabiilsust. Seejärel teostati elektroonilise olekutiheduse (DOS) ja optiliste omaduste arvutused. Arvutatud foononi dispersioonid ei sisalda imaginaarsagedusi, kinnitades, et optimeeritud struktuur on dünaamiliselt stabiilne. Elektroonilise struktuuri arvutused näitavad isoleerivat käitumist laia keelutsooniga. Optiliste arvutuste tulemusena saadi YHO dielektriline funktsioon ja neeldumisspekter. Arvutatud optiline neeldumisspekter on kooskõlas olemasolevate eksperimentaalsete andmetega. Peamised tulemused hõlmavad optimeeritud kristallgeomeetriat, foonondispersioone, DOS-i ja ütriumoksühüdriidi optilisi spektreid.

Appendices

Appendix A. Translation vectors of the face-centered cubic lattice

Symmetry-equivalent atomic positions in fcc structures can be generated using the translation vectors

$$(0,0,0), \quad \left(0,\tfrac{1}{2},\tfrac{1}{2}\right), \quad \left(\tfrac{1}{2},0,\tfrac{1}{2}\right), \quad \left(\tfrac{1}{2},\tfrac{1}{2},0\right). \tag{12}$$

The application of these translations to the atomic positions of the primitive-cell representation generates the corresponding conventional fcc unit cell.

Appendix B POSCAR files

B.1 Constructed structure POSCAR file

```
YHO primitive, F-43m (#216), constructed (comment)
 1.0
 0.0  2.6  2.6
 2.6  0.0  2.6
 2.6  2.6  0.0
Y    H    O
1    1    1
Direct
 0.25  0.25  0.25
 0.00  0.00  0.00
 0.50  0.50  0.50
```

B.2 Optimised structure POSCAR file

```
YHO primitive, F-43m (#216), optimised (comment)
 1.00000000000000
 0.0000000000000000    2.6468137473511777    2.6468137473511777
 2.6468137473511777    0.0000000000000000    2.6468137473511777
 2.6468137473511777    2.6468137473511777    0.0000000000000000
Y    H    O
1    1    1
Direct
 0.2500000000000000  0.2500000000000000  0.2500000000000000
 0.0000000000000000  0.0000000000000000  0.0000000000000000
 0.5000000000000000  0.5000000000000000  0.5000000000000000
```

Appendix C INCAR files used in calculations

General settings common to all calculations (unspecified parameters were set to default *VASP* values):

- `NELM = 60` (maximum number of SCF iterations)
- `NSW = 0` corresponds to static calculations (no ionic relaxation)
- For `ISMEAR = -5`, the parameter `SIGMA` is not used

The INCAR files listed below were used at different stages of the computational workflow.

C.1 PBE geometry optimisation (relaxation)

```
GGA    = PE          # PBE functional
ENCUT  = 700         # plane-wave energy cutoff (high accuracy)
PREC   = Accurate    # precision level for FFT grids and integrals

EDIFF  = 1E-7        # electronic SCF convergence criterion (energy)
EDIFFG = -0.005      # ionic convergence criterion (forces, eV/Å)

NBANDS = 48          # number of bands (tripled default value NBANDS = 16)

NSW    = 30          # maximum number of ionic steps
IBRION = 2           # ionic relaxation algorithm (conjugate gradient)
ISIF   = 3           # relax ions, cell shape, and volume

ISMEAR = 0           # Gaussian smearing
SIGMA  = 0.05        # smearing width (eV)

LREAL  = .FALSE.     # projection in reciprocal space (higher accuracy)
LASPH  = .TRUE.      # include non-spherical contributions inside PAW spheres
ADDGRID= .TRUE.      # finer FFT grid (to reduce numerical noise)

LWAVE  = .FALSE.     # do not write WAVECAR (not needed for relax)
LCHARG = .FALSE.     # do not write CHGCAR (not needed for relax)
```

C.2 Phonon force calculation for displaced supercells (PBE, using *phonopy*)

```
GGA    = PE          # PBE functional
```

```
ENCUT  = 700         # plane-wave energy cutoff
PREC   = Accurate    # high-precision FFT grids and integrals

EDIFF  = 1E-8        # tight electronic convergence (for accurate forces)

NBANDS = 48          # number of bands (tripled default value)

NSW    = 0           # no ionic relaxation (zero ionic steps)

ISMEAR = 0           # Gaussian smearing (for stable force evaluation)
SIGMA  = 0.05        # smearing width (eV)

LREAL  = .FALSE.     # projection in reciprocal space
LASPH  = .TRUE.      # non-spherical PAW contributions
ADDGRID= .TRUE.      # finer FFT grid

LWAVE  = .FALSE.     # do not write WAVECAR
LCHARG = .FALSE.     # do not write CHGCAR

ISYM   = 0           # disable symmetry for displaced structures
```

C.3 PBE static electronic structure + DOS

```
GGA    = PE          # PBE functional
ENCUT  = 700         # plane-wave energy cutoff
PREC   = Accurate    # high-precision FFT grids and integrals

EDIFF  = 1E-7        # electronic SCF convergence criterion (energy)

NBANDS = 48          # number of bands (tripled default value)

NSW    = 0           # no ionic relaxation (zero ionic steps)

ISMEAR = -5          # tetrahedron method for accurate DOS

NEDOS  = 2000        # number of DOS energy points
LORBIT = 11          # projected DOS (PDOS)

LREAL  = .FALSE.     # projection in reciprocal space
LASPH  = .TRUE.      # non-spherical PAW contributions
ADDGRID= .TRUE.      # finer FFT grid
```

```
LWAVE  = .TRUE.      # write WAVECAR for next calculations
LCHARG = .TRUE.      # write CHGCAR for next calculations
```

C.4 HSE06 static electronic structure + DOS

```
ISTART = 1           # read previously created WAVECAR (from PBE static + DOS)
ICHARG = 1           # read previously created CHGCAR (from PBE static + DOS)

ENCUT  = 700         # plane-wave energy cutoff
PREC   = Accurate    # high-precision FFT grids and integrals

EDIFF    = 1E-7      # electronic SCF convergence criterion (energy)

NBANDS   = 48        # number of bands (tripled default value)

NSW      = 0         # no ionic relaxation (zero ionic steps)

ISMEAR   = -5        # tetrahedron method for accurate DOS

NEDOS    = 2000      # number of DOS energy points
LORBIT   = 11        # projected DOS (PDOS)

LREAL    = .FALSE.   # projection in reciprocal space
LASPH    = .TRUE.    # non-spherical PAW corrections
ADDGRID  = .TRUE.    # finer FFT grid

LWAVE    = .TRUE.    # write WAVECAR
LCHARG   = .TRUE.    # write CHGCAR

# Hybrid functional (HSE06)
LHFCALC  = .TRUE.    # enable hybrid functional
AEXX     = 0.25      # exact exchange fraction
HFSCREEN = 0.2       # screening parameter
ALGO     = D         # algorithm for hybrid calculations
PRECFOCK = Normal    # precision for Fock exchange
```

C.5 HSE06 optical properties calculations (static SCF + optics)

```
ISTART   = 1         # read previously created WAVECAR (from HSE static + DOS)
ICHARG   = 1         # read previously created CHGCAR (from HSE static + DOS)

ENCUT    = 700       # plane-wave energy cutoff
```

```
PREC     = Accurate    # high-precision FFT grids and integrals

EDIFF    = 1E-7        # SCF convergence

NSW      = 0           # no ionic relaxation

ISMEAR   = 0           # Gaussian smearing (more stable SCF than -5)
SIGMA    = 0.05        # smearing width (eV)

# Optics
LOPTICS  = .TRUE.      # enable optical properties (dielectric function)
NEDOS    = 2000        # energy grid for optical spectra
NBANDS   = 48          # number of bands (tripled default value)

LREAL    = .FALSE.     # projection in reciprocal space
LASPH    = .TRUE.      # non-spherical PAW corrections
ADDGRID  = .TRUE.      # finer FFT grid

LWAVE    = .FALSE.     # do not write WAVECAR
LCHARG   = .TRUE.      # write CHGCAR

# Hybrid functional (HSE06)
LHFCALC  = .TRUE.      # enable hybrid functional
AEXX     = 0.25        # exact exchange fraction
HFSCREEN = 0.2         # screening parameter
ALGO     = D           # algorithm for hybrid calculations
PRECFOCK = Normal      # precision for Fock exchange
```

Appendix D KPOINTS files used in calculations

All KPOINTS files were generated using the same scheme (Gamma-centered Monkhorst-Pack grid):

```
Regular k-point mesh
0              ! number of k points is determined automatically
Gamma          ! Gamma centered mesh
N1 N2 N3       ! subdivisions along the reciprocal lattice vectors
0  0  0        ! no shift of the mesh
```

The following k-point meshes (`N1 N2 N3`) were used for different calculations:

- PBE geometry optimisation (relaxation): $6 \times 6 \times 6$
- Phonon force calculations for displaced supercells (PBE, using *phonopy*): $3 \times 3 \times 3$ mesh for a $2 \times 2 \times 2$ supercell (equivalent to a $6 \times 6 \times 6$ mesh in the primitive cell)
- PBE static electronic structure and DOS: $6 \times 6 \times 6$
- HSE06 static electronic structure and DOS: $6 \times 6 \times 6$
- HSE06 optical properties:
  - for YHO, convergence was tested using $6 \times 6 \times 6$ and $10 \times 10 \times 10$ meshes, the final calculations were performed using the $10 \times 10 \times 10$ mesh,
  - for LaHO, a $6 \times 6 \times 6$ mesh was used

Appendix E Additional calculations

This appendix presents additional calculations performed for selected rare-earth and transition-metal oxyhydride structures: LaHO, NdHO, NbHO, ZrHO, all belonging to the space group $F\bar{4}3m$. Of these structures, only lanthanum oxyhydride was found to be dynamically stable. From its DOS graph, it can be seen that LaHO exhibits insulating behaviour, similarly to YHO.

E.1 Lanthanum oxyhydride calculations

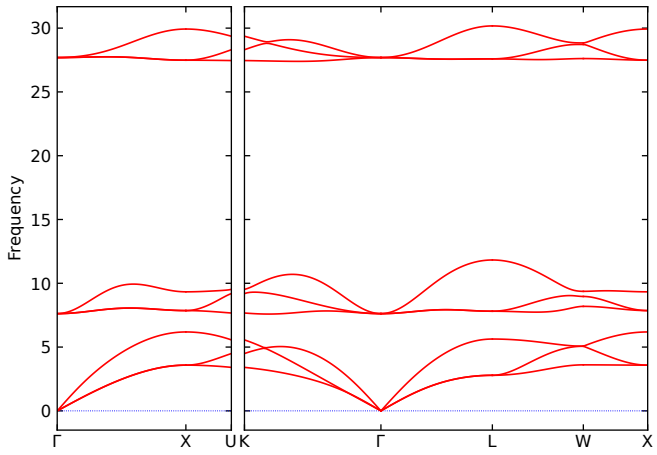

Figure 10: Phonon dispersion relations calculated for the optimized LaHO structure.

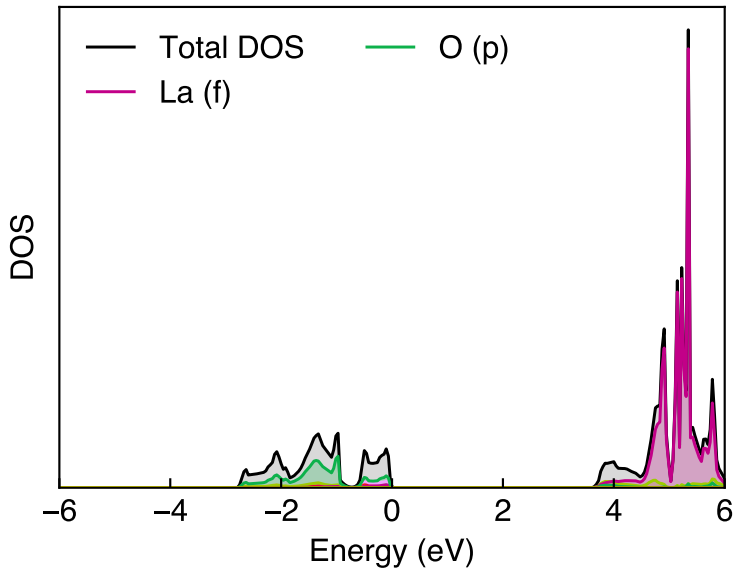

Figure 11: PBE DOS for the LaHO structure.

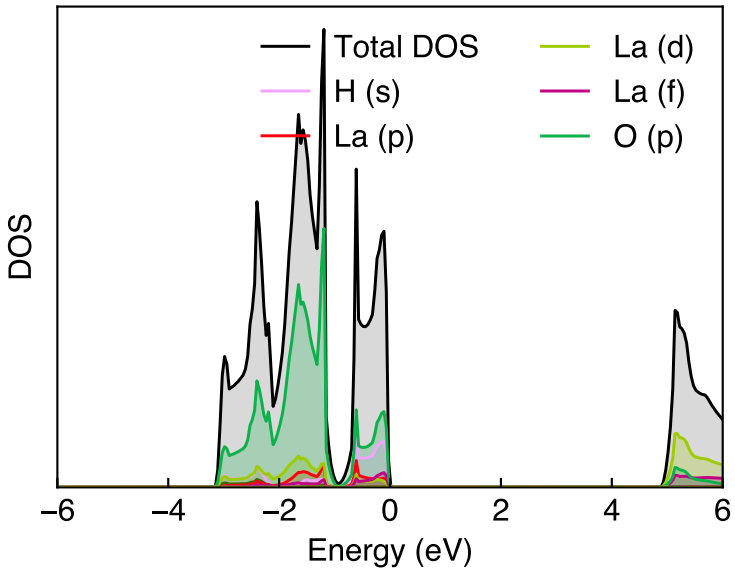

Figure 12: HSE06 DOS for the LaHO structure.

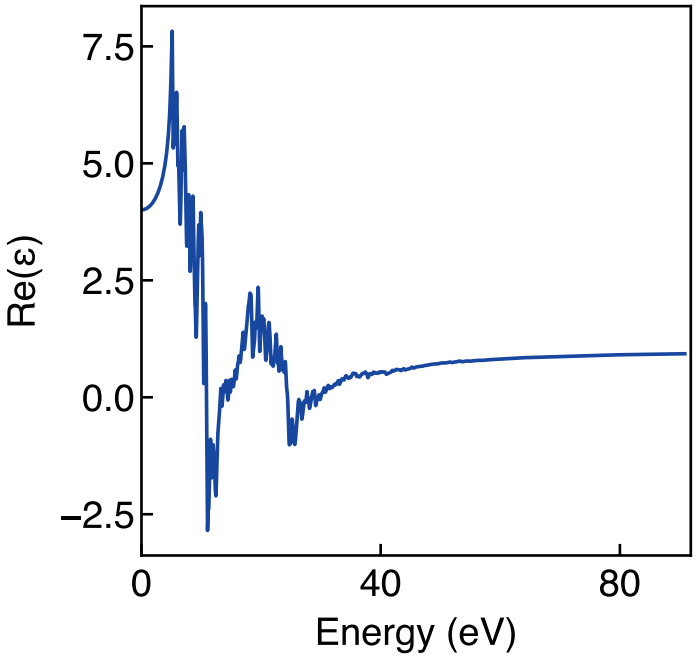

Figure 13: Real part of the dielectric function for the LaHO structure.

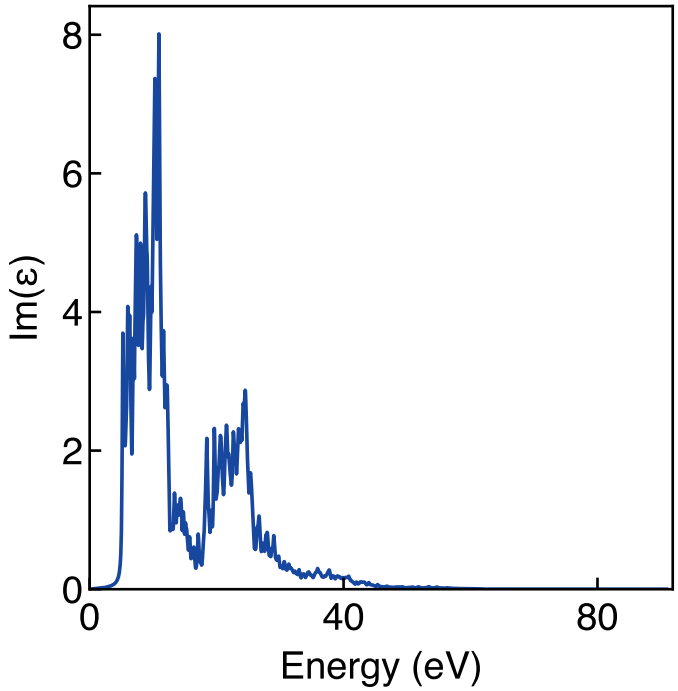

Figure 14: Imaginary part of the dielectric function for the LaHO structure.

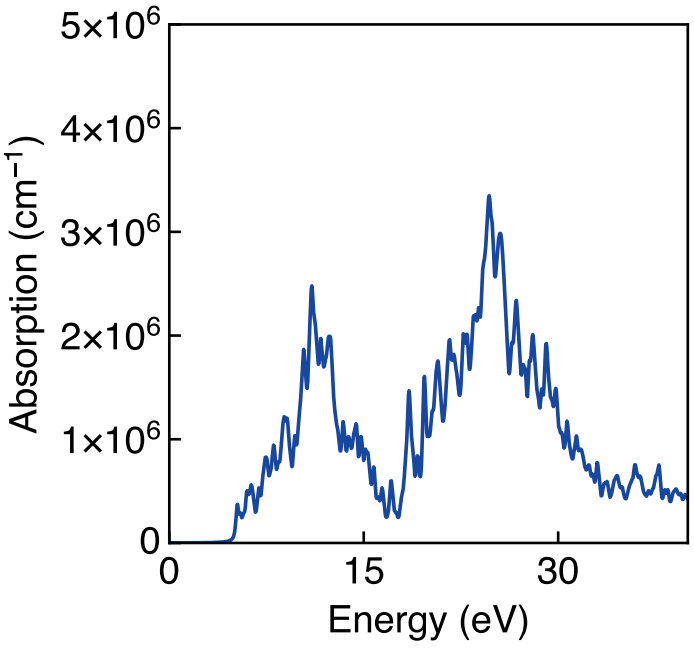

Figure 15: Optical absorption spectrum of the LaHO structure.

E.2 Neodymium oxyhydride calculations

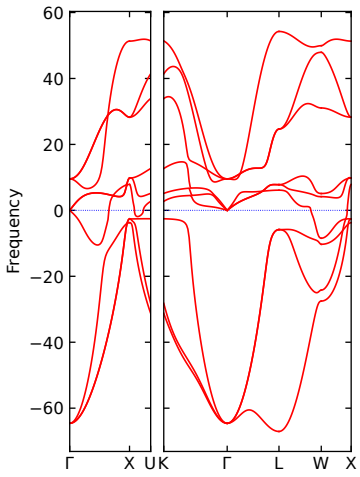

Figure 16: Phonon dispersion relations calculated for the optimized NdHO structure. Imaginary frequencies (shown as negative values) indicate dynamical instability.

E.3 Niobium oxyhydride calculations

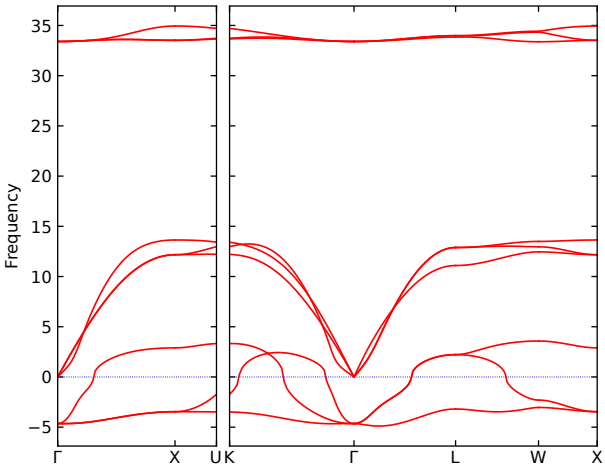

Figure 17: Phonon dispersion relations calculated for the optimized NbHO structure.

E.4 Zirconium oxyhydride calculations

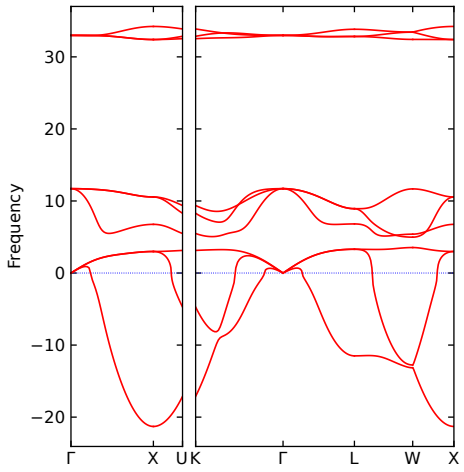

Figure 18: Phonon dispersion relations calculated for the optimized ZrHO structure.

Annex
to Rector's directive No 1-8/17 of 7 April 2020

Non-exclusive licence for reproduction and publication of a graduation thesis[1]

I Ivan Novoseltsev

1. grant Tallinn University of Technology free licence (non-exclusive licence) for my thesis "Crystal structure prediction and first-principles investigation of the vibrational, electronic, and optical properties of yttrium oxyhydride",

supervised by Mihhail Klopov and Smagul Karazhanov,

1.1 to be reproduced for the purposes of preservation and electronic publication of the graduation thesis, incl. to be entered in the digital collection of the library of Tallinn University of Technology until expiry of the term of copyright;

1.2 to be published via the web of Tallinn University of Technology, incl. to be entered in the digital collection of the library of Tallinn University of Technology until expiry of the term of copyright.

2. I am aware that the author also retains the rights specified in clause 1 of the non-exclusive licence.

3. I confirm that granting the non-exclusive licence does not infringe other persons' intellectual property rights, the rights arising from the Personal Data Protection Act or rights arising from other legislation.

24.05.2026

[1] *The non-exclusive licence is not valid during the validity of access restriction indicated in the student's application for restriction on access to the graduation thesis that has been signed by the school's dean, except in case of the university's right to reproduce the thesis for preservation purposes only. If a graduation thesis is based on the joint creative activity of two or more persons and the co-author(s) has/have not granted, by the set deadline, the student defending his/her graduation thesis consent to reproduce and publish the graduation thesis in compliance with clauses 1.1 and 1.2 of the non-exclusive licence, the non-exclusive license shall not be valid for the period.*